JOC The Journal of Organic Chemistry

pubs.acs.org/joc Article

Olive-Shaped Organic Cages: Synthesis and Remarkable Promotion of Hydrazone Condensation through Encapsulation in Water

Yan-Yan Xu, Hong-Kun Liu, Ze-Kun Wang, Bo Song, Dan-Wei Zhang,* Hui Wang, Zhiming Li,* Xiaopeng Li, and Zhan-Ting Li*

Cite This: J. Org. Chem. 2021, 86, 3943−3951 Read Online

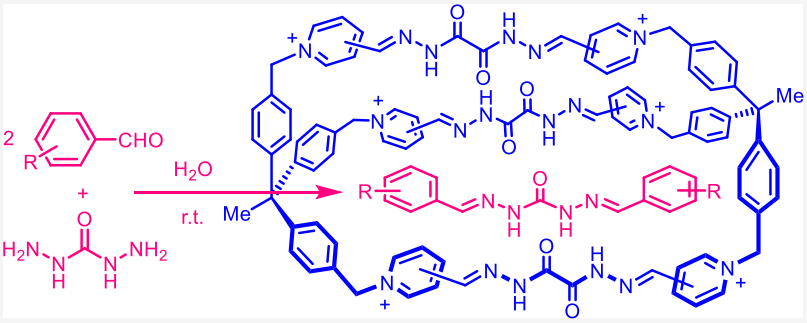

ABSTRACT: Two organic cages have been prepared in situ in water through the 2 + 3 hydrazone coupling of two pyridinium-derived trialdehydes and oxalohydrazide. The highly water-soluble cages encapsulate and solubilize linear neutral molecules. Such encapsulation has been applied for the promotion of both two- or three-component hydrazone condensation in water. For two-component reactions, the yields of the resulting monohydrazones are increased from 5−10 to 90−96%. For three-component reactions of hydrazinecarbohydrazide with 11 aromatic aldehydes, in the presence of the organic cages, the bihydrazone products can be produced in 88−96% yields. In contrast, without the promotion of the organic cages, 9 of the reactions do not afford the corresponding dihydrazone product.

■ INTRODUCTION

Molecular cages provide unique microenvironments for the exploitation of molecular recognition and chemical transformations in a confined space.[1] The construction of molecular cages has been realized mainly in a stepwise synthetic manner through the formation of relatively strong, irreversible bonds,[2] such as amides or C−C bonds, which is often accompanied by a low yield for the last step of macrocyclization.[3] The utilization of dynamic covalent chemistry (DCC) has allowed for the generation of molecular cages in higher or even quantitative yields.[4] Nevertheless, most of the reported structures of this category have been achieved in organic solvents.[5] The development of efficient DCC approaches for the self-assembly of molecular cages in water, the highly polar medium of biology, has only gained limited success,[6] whereas the potential of water-compatible organic cages for the enhancement or catalysis of chemical transformations in water has been rarely explored, even though macrocycles and cages constructed by the metal−ligand coordination-driven self-assembly have been extensively investigated.[7]

Quantitative formation of the hydrazone bonds from rigid tritopic precursors represents an efficient strategy for the construction of covalent organic frameworks.[8] In contrast, flexible tritopic building blocks have also found important applications in the fabrication of hollow supramolecular capsules in organic solvents.[2j,3,5,6a] We have utilized the pyridinium unit to provide water solubility for both supramolecular and covalent organic networks from tetraphenylmethane-based precursors.[9] Given that pyridinium-incorporated organic macrocycles and cages can be generated in water through hydrazone or oxime condensation,[10,11] we envisioned that triphenylmethane-cored tripyridinium derivatives might be used as precursors for the construction of new water-soluble organic cages. Herein, we describe the construction of two olive-like organic cages through the 2 + 3 condensation of tritopic pyridinium-based trialdehydes and diacylhydrazines in water. We further demonstrate that the new water-soluble cages can remarkably promote two- and three-component hydrazone condensation through efficient encapsulation of the resulting linear uni- and bihydrazone products.

Received: November 21, 2020
Published: February 18, 2021

https://dx.doi.org/10.1021/acs.joc.0c02792
J. Org. Chem. 2021, 86, 3943−3951

Scheme 1. Synthesis of Organic Cages C1 and C2 and the Structure of Guest G1

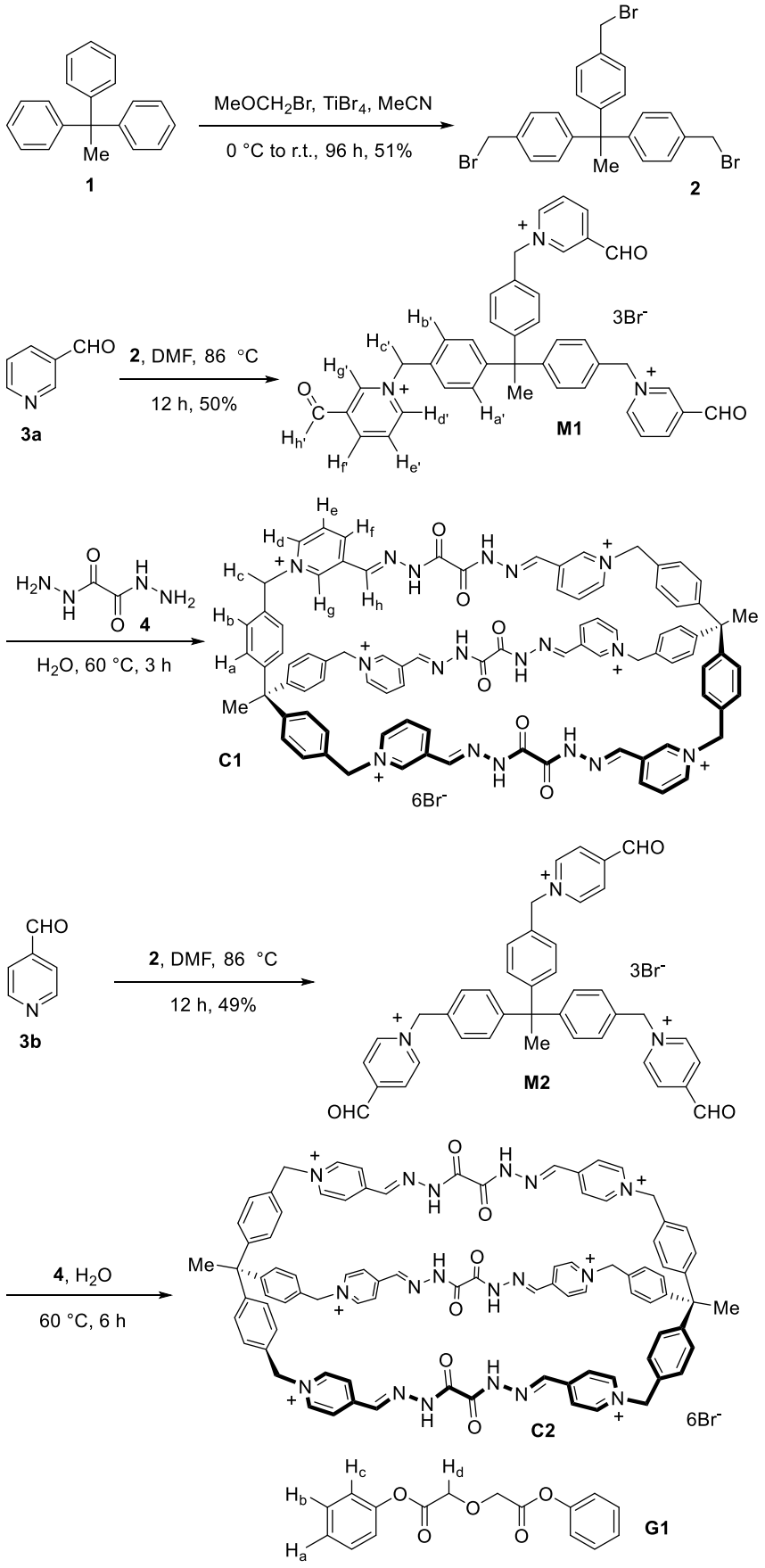

https://dx.doi.org/10.1021/acs.joc.0c02792
J. Org. Chem. 2021, 86, 3943−3951

RESULTS AND DISCUSSION

Compounds **C1** and **C2** were designed as water-soluble organic cages for the encapsulation of molecular guests and possible further application for the promotion of organic reactions in water. Their synthetic routes are shown in Scheme 1. Compound **1** first reacted with bromomethyl methyl ether in the presence of titanium bromide in dichloromethane to afford tribromide **2** in 51% yield.[12] Treatment of **2** with nicotinaldehyde **3a** or isonicotinaldehyde **3b** in DMF produced trialdehydes **M1** and **M2** in 50 or 49% yield. Finally, the two intermediates reacted with highly soluble oxalohydrazide **4** (2:3) in water at 60 °C to generate **C1** or **C2**, respectively. Both **M1** and **M2** had a high water-solubility (≥30 mM). ^{1}H NMR in D_2O showed that because of the strong electron-withdrawing effect of the pyridinium, about 95% of the C*H*O group of **M1** was hydrated to afford C*H*$(OH)_2$ (Figure 1), which was

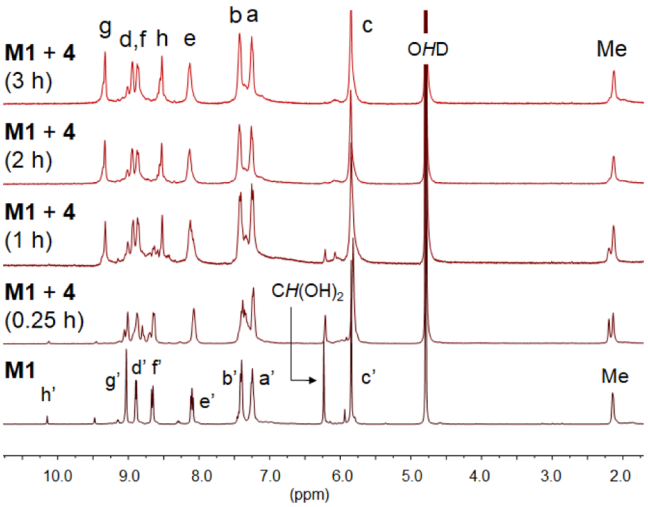

Figure 1. ^{1}H NMR spectra (400 MHz) of the 2:3 mixture of **M1** (10 mM) and **4** (15 mM) in D_2O at 60 °C after 0.25, 1, 2, and 3 h, which illustrates the formation of molecular cage **C1** from the condensation of **M1** and **4** after 3 h.

evaluated by comparing the ratio of the integral intensity of the two signals at 10.1 and 6.2 ppm, respectively, whereas the hydration of the C*H*O group was quantitative for **M2** (Figure S1). In contrast, their ^{1}H NMR spectra in DMSO-d_6 exhibited the signals of both C*H*O and C*H*$(OH)_2$ units, with the latter being 11 and 61%, respectively (Figures S2 and S3). At the concentration of 10 mM, the reactions of **M1** and **M2** with **4** (15 mM) in D_2O were complete after about 3 or 6 h, as revealed by the ^{1}H NMR spectra which indicated that the diagnostic signals of the C*H*O and C*H*$(OH)_2$ groups of **M1** and **M2** disappeared completely. The formation of **C1** and **C2** was first evidenced by their ^{1}H NMR spectra (Figures 1 and S1), which exhibited one set of broad signals. The signals in the downfield area could be assigned through their 2D ^{1}H COSY spectrum (Figures S4 and S5). The mass spectra of the two samples exhibited peaks which were consistent with the cage structures (Figures S6). Compound **C1** displayed strong peaks corresponding to $[M - 6Br - 2H]^{4+}$ (m/z: 370.15) and $[M - 6Br - 3H]^{3+}$ (m/z: 493.20), whereas **C2** gave rise to peaks that were related to $[M - 6Br + MeOH - H]^{5+}$ (m/z: 302.75), $[M - 6Br + MeOH - 2H]^{4+}$ (m/z: 378.18), and $[M - 6Br - 3H + H_2O]^{3+}$ (m/z: 499.57). Upon evaporation of the solvent under reduced pressure, the resulting solids became insoluble in water at room temperature. ^{1}H NMR spectra in D_2O showed that, at higher temperature (>50 °C), the solids dissolved slowly to afford the cage molecules again.

Dynamic light scattering (DLS) experiments in water revealed the formation of only one small entity with a hydrodynamic diameter (D_H) of approximately 1.3 nm for both the samples even at a very high concentration ([**M1**] = [**M2**] = 10 mM) (Figure 2), whereas **M1** and **M2** of the same concentration

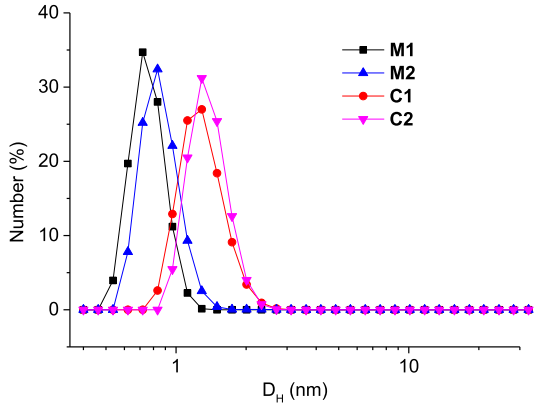

Figure 2. DLS profiles of the solution of **M1**, **M2**, **C1**, and **C2** ([**M1**] = [**M2**] = 10 mM) in water at 25 °C.

afforded even smaller D_H values (<0.7 nm). These results were consistent with the size of the olive-shaped organic cages of **C1** and **C2** and the selective formation of the proposed cages. Thus, the complexity of the ^{1}H NMR spectra of **C1** and **C2** might be attributed to the existence of different conformers as a result of the rigidity of the backbones. Heating the solution to 80 °C notably increased the resolution of the ^{1}H NMR spectra of **C1** and **C2** (Figures S7 and S8). Even at 80 °C, both spectra did not exhibit the signal of the C*H*$(OH)_2$ group. Diluting the solution from [**M1**] = [**M2**] = 5 mM to [**M1**] = [**M2**] = 0.5 mM did not lead to an observable signal of the C*H*$(OH)_2$ group (Figures S9 and S10), suggesting high stability of the two organic cages in water.

To get a deep insight into the conformational isomers of **C1** and **C2**, we further conducted molecular modeling studies for both cages using the density functional theory method. B3LYP computations were carried out using Gaussian 09 software package.[13,14] Because of the large size of the structures, small basis sets 3-21G were used. Truhlar's SMD solvation model was employed to consider the solvent effect (water).[15] The other calculation details are provided in the Supporting Information. It was found that the rigidity of the dihydrazone linkers and the rotation hindrance of the $H_2C-N(py)$ bonds led to the formation of multiple low-energy cage conformers (Figures 3 and S11 and Table S1). For both the molecules, interconversions between different low-energy conformations do not occur, which indicate the existence of high energy barriers and may account for the complicated signal patterns of their ^{1}H NMR spectra. In both the molecules, the central linkers are almost perfect planar. The relative energies of the three conformers of **C1** are 0.0, 0.5, and 1.2 kcal/mol. Two of the three linker planes of the first conformer are nearly parallel to each other, whereas the remaining one is perpendicular to the two formers. For the second conformer, the three chains are distorted into S-shape because of the $H_2C-N(py)$ bond rotation, while the plane of the three linkers of the third one is roughly parallel with the benzyl

https://dx.doi.org/10.1021/acs.joc.0c02792
J. Org. Chem. 2021, 86, 3943−3951

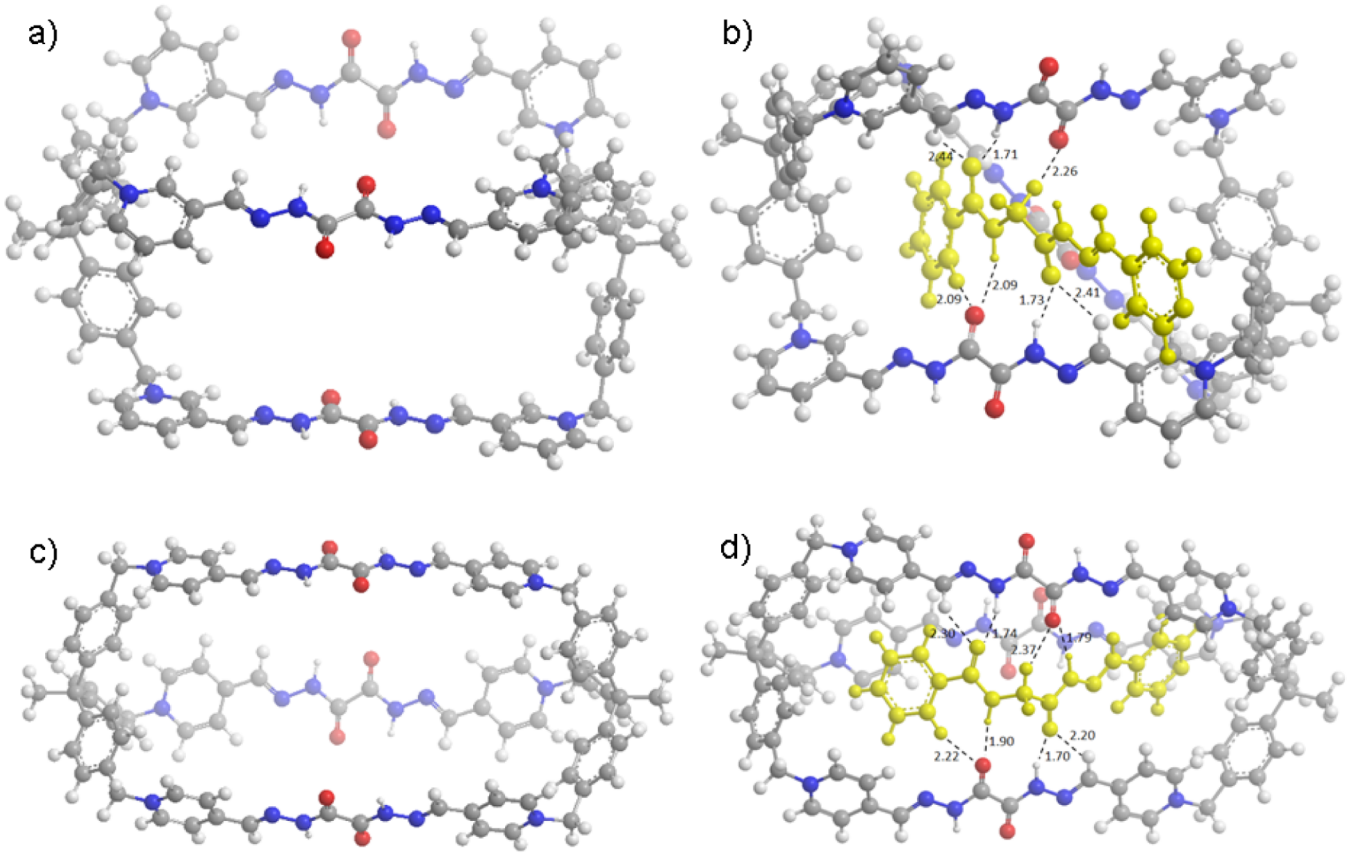

Figure 3. Lowest-energy conformers of (a) **C1-1**, (b) complex **C1** ⊂ **7b-1**, (c) **C2-1**, and (d) complex **C2** ⊂ **7b-1**. The numbers are the lengths of hydrogen bonds in Å.

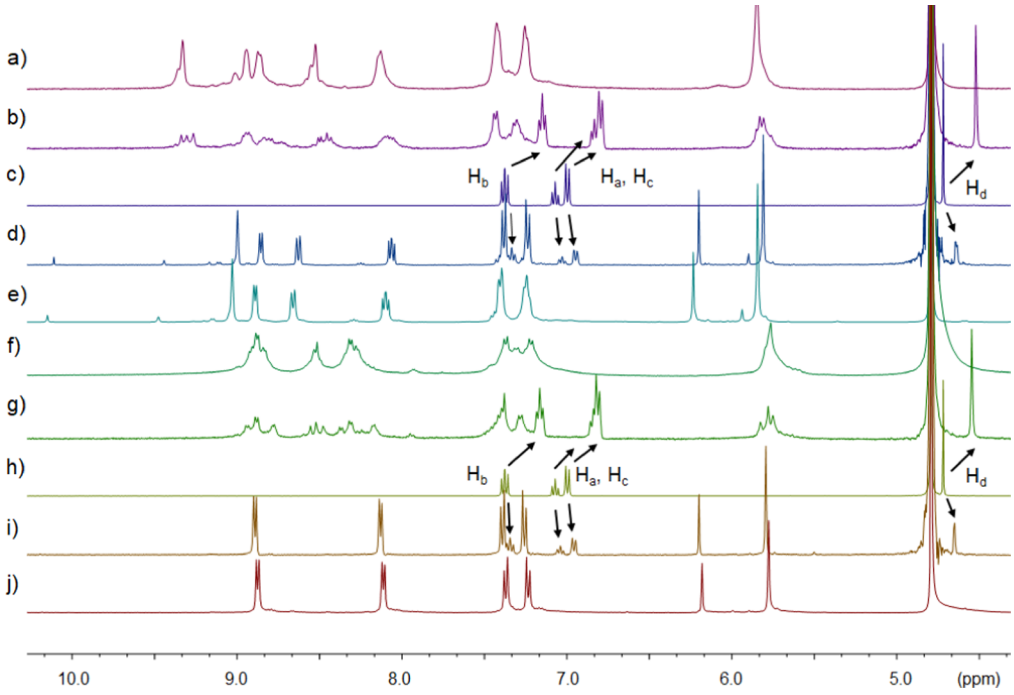

Figure 4. Partial ^{1}H NMR of (a) **C1**, (b) **G1** + **C1**, (c) **G1**, (d) **M1** + **G1**, (e) **M1**, (f) **C2**, (g) **C2** + **G1**, (h) **G1**, (i) **M2** + **G1**, and (j) **M2** ([**C1**] = [**C2**] = [**G1**] = 1.25 mM, [**M1**] = [**M2**] = 2.5 mM) in D_2O at 25 °C.

moieties that connect them. In contrast, the difference of the conformers of **C2** is quite small, which is mainly caused by the relative orientation of the pyridinium units.

The inclusion of **C1** and **C2** was then investigated with commercially available, linear **G1** (Scheme 1) as a guest. **G1** was soluble in water but also generally hydrophobic. Compared with

https://dx.doi.org/10.1021/acs.joc.0c02792
J. Org. Chem. 2021, 86, 3943−3951

Scheme 2. Molecular Cage-Promoted Reactions of 5 with 6a and 6b in Water[a]

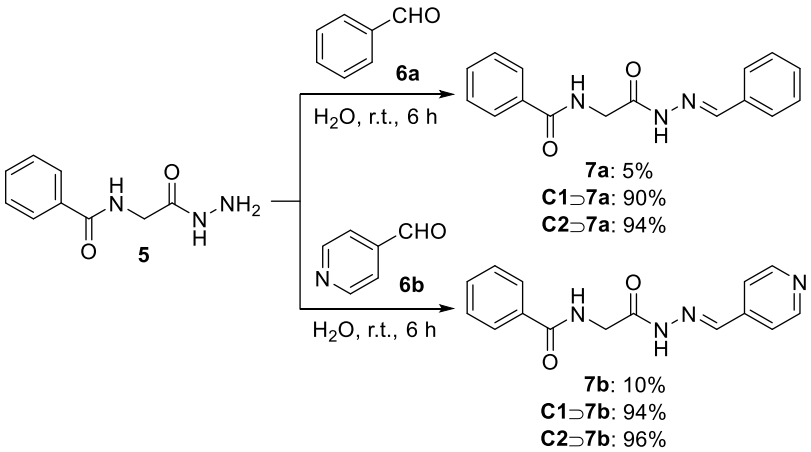

[a][C1] = [C2] = [5] = [6a,b] = 1.25 mM. The yield of the products was determined by HPLC.

the corresponding signals of **G1**, the signals of the H-a−d protons of **G1** in D_2O in the 1:1 mixture with **C1** shifted upfield by 0.23, 0.23, 0.18, and 0.18 pm, respectively (Figure 4). In contrast, all the signals of **G1** in the solution of its 1:2 mixture with **M1** underwent much smaller shifting (≤0.08 ppm) (Figure 4). Similar results were also observed for **G1** with **C2**. Thus, we proposed that both **C1** and **C2** were capable of encapsulating **G1**. The Job plot further supported that the encapsulation of **G1** by **C1** and **C2** was in a 1:1 stoichiometry (Figure S12).[6a] The larger upfield shifting of the H-a and H-b signals of **G1**, as compared with that of its H-c and H-d signals, also suggested that the guest adopted an extended conformation inside the cage of the host, and thus the H-a and H-b protons suffered the strongest shielding of the triphenylmethyl moiety of the host. Diffusion-ordered spectroscopic experiments were further conducted for the solution of **C2**, **G1**, and their 1:1 mixture in D_2O. The diffusion coefficient (D) of the two species in their respective pure solution was determined to be 1.4×10^{-6} and 5.9×10^{-6} cm^2/s, while their mixture afforded the identical D of 1.4×10^{-6} cm^2/s for both the compounds (Figure S13). The fact that the D value of **G1** was decreased to the level of **C2** solidly supported that it was encapsulated by **C2**. ^{1}H NMR titration experiments were then conducted (Figures S14 and S15). By using a nonlinear regression fitting, the 1:1 binding pattern with the change of the chemical shifting of H-d (CH_2) of **G1** as the probe, we determined the association constant (K_a) of the 1:1 complexes formed between **G1** and the two cages to be 2.2 (±0.4) × 10^3 and 1.6 (±0.3) × 10^3 M^{-1}. As the encapsulation for the neutral **G1** occurred in water, the main driving force should come from hydrophobicity.[16] Through the titration experiments (Figures S14 and S15), the H-d of **G1** displayed a signal of high resolution, which also supported that the host and guest were in fast exchange.

Given the efficient encapsulation of **C1** and **C2** for linear guest **G1**, we envisioned that the new cages **C1** and **C2** might stabilize the molecules of similar size and length in water through efficient encapsulation. To test this hypothesis, we first investigated the reactions between acylhydrazine **5** and aldehydes **6a** and **6b**. At the concentration of 1.25 mM for all the substrates, the two reactions gave rise to hydrazones **7a** and **7b** only in 5 and 10% yields in water that contained 7.5 mM of KBr which had the identical ion concentration as the systems of **C1** and **C2** (Scheme 2). However, in the presence of **C1** and **C2** of the same concentration, compound **7a** could be formed in 90 or 94% yield, whereas the yield of compound **7b** was increased to 94 or 96%. The ^{1}H NMR spectra of the two 1:1 mixtures in D_2O showed that the signals of the mixtures changed considerably (Figures S17 and S18) compared with the respective spectrum of **C1** and the hydrazones, which supported the fact that important interactions occurred between the organic cages and the two hydrazones. In the presence of **C1** (1.25 mM), the reaction of **5** and **6b** (1:1) was also conducted at higher concentrations of the substrates (2.5 and 5.0 mM), which gave rise to **7b** in 93 and 96% yields, respectively, which were comparable to that obtained at the substrate concentration of 1.25 mM (94%). Thus, the promotion of the hydrazine bond in the molecular cage did not suffer from product inhibition. As **7b** was formed in higher yield in the presence of **C1** or **C2**, isothermal titration calorimetric experiments were conducted in water for evaluating the encapsulation of **7b** by **C1** and **C2** (Figures S19 and S20), which afforded a K_a of 5.8 (±0.5) × 10^4 and 4.4 (±0.7) × 10^4 M^{-1} for their 1:1 complexes. The values were even higher than that of the complex formed by **G1** and **C1** or **C2**, which might be attributed to the higher rigidity of **7b** as compared with **G1**. The corresponding enthalpy changes (ΔH) of the two complexes were −3.12 (±0.14) and −4.69 (±0.43) kcal/mol, whereas their entropy changes ($-T\Delta S$) were −3.37 and −1.63 kcal/mol. Thus, the formation of the first complex was driven both enthalpically and entropically. For the second one, the entropy contribution played the major role.

The above promotion of organic cages **C1** and **C2** for hydrazone condensation was further applied for the three-component reactions of **6a−k** with **8** in water (Scheme 3), which afforded dihydrazones **9a−k** and hydrazones **10a−k**. In the absence of **C1** or **C2**, the reactions of **6a−k** with **8** afforded hydrazone derivatives **10a−k** as the major products, all in low yields (4−19%) (Table 1). Moreover, except for the reactions of **6c** and **6d**, which produced dihydrazone **9c** or **9d** both in 6% yield, all the other reactions did not give rise to the corresponding dihydrazone product in an observable yield. However, in the presence of **C1** or **C2**, all the reactions gave rise to the dihydrazone product in high to excellent yields (88−96%) (Table 1). Consistently, the yield of the monohydrazone derivatives decreased to 2−9%. It is reasonable to assume that the hydrazone bond of the same series of mono- and dicondensation products were comparable. Thus, the formation

https://dx.doi.org/10.1021/acs.joc.0c02792
J. Org. Chem. 2021, 86, 3943−3951

Scheme 3. Molecular Cage-Promoted Reactions of 6a−k with 8 in Water[a]

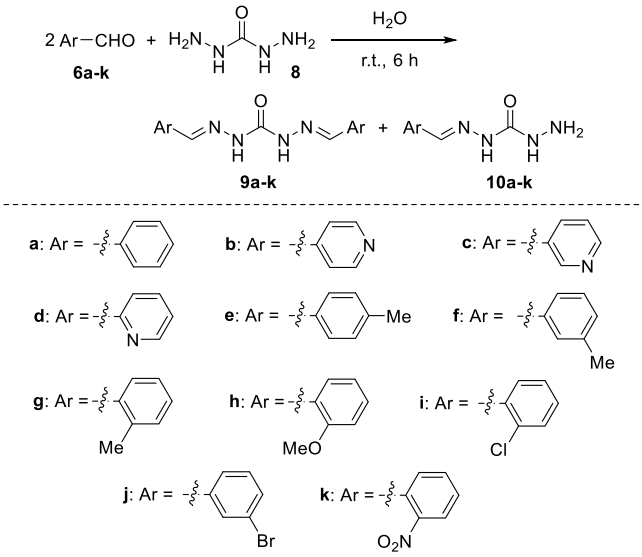

[a][**C1**] = [**C2**] = [**8**] = 1.25 mM. [**6a−k**] = 2.5 mM. The yield of the products was determined by HPLC.

of the dihydrazones in high yields in the presence of **C1** or **C2** should be attributed to the efficient encapsulation of the organic cages for the linear dihydrazones. The lower yield of **10a−k** in the presence of the two molecular cages also suggested that these shorter molecules were not efficiently encapsulated probably owing to structural mismatching. It is noteworthy that, although both the organic cages and the guests were hydrazone derivatives, the fact that the linear mono- and dihydrazones could be generated inside the organic cages suggests that the two species possessed good orthogonality.

Molecular modeling studies for the encapsulation of **7b** by **C1** and **C2** also revealed multiple low-energy conformations of the 1:1 complexes, with the guest being orientated in the cavity of the two hosts (Figures 3 and S11). The computed complexes also showed the existence of intermolecular hydrogen bonds, which should combine with the hydrophobicity, mainly occurring between the triphenylmethane moieties of the cage and the aromatic units of the guest, to stabilize the encapsulation complexes.

Finally, the effect of **C1** and **C2** on the solubility of all the linear hydrazone derivatives in water was investigated (Table S2). It was found that both **C1** and **C2** were able to enhance the solubility of all the hydrazones. The water solubility of the hydrazones was quite different depending on the polarity of the aromatic units. However, at [**C1**] = [**C2**] = 1.25 mM, their solubility increased to 1.1−1.2 mM, which may be attributed to the formation of the 1:1 encapsulation complexes.

■ CONCLUSIONS

We have demonstrated that organic cages can be constructed in situ in water through the formation of multiple hydrazone bonds from rationally designed molecular precursors. The new organic cages can efficiently encapsulate the linear molecular guests driven by hydrophobicity and enhance their water solubility through encapsulation. The encapsulation remarkably improves the formation of linear products from two- or three-component reactions of aldehyde and acylhydrazine precursors in water, with the yield being increased from zero to 88−96%. The results described herein well illustrate the importance of the structural matching for host−guest systems in water. By introducing chiral linkers, new chiral organic cages may be constructed, which will allow for the investigation of the stereoselectivity of the reactions of the chiral substrates. Large molecular cages are expected to encapsulate long, folded linear molecules in water, which may be utilized to promote intramolecular reactions to produce giant macrocycles.

■ EXPERIMENTAL SECTION

General Methods. All reagents and solvents were purchased from commercial sources and used without further purification. All the reactions were conducted under the N_2 atmosphere. Nuclear magnetic resonance (NMR) spectra were recorded using Bruker AVANCE III 400 spectrometers, with working frequencies of 400 and 100 MHz for ^{1}H and ^{13}C, respectively. Chemical shifts are reported in ppm relative to the residual internal nondeuterated solvent signals (D_2O: δ = 4.79 ppm). High-resolution mass spectra (HRMS) were recorded on Fourier transform ion cyclotron resonance mass spectrometry. DLS experiments were conducted on a Malvern Zetasizer Nano ZS90 using a monochromatic coherent He−Ne laser (633 nm) as the light source and detector that detected the scattered light at an angle of 90°. The thermodynamic parameters and association constants were determined by titration calorimetry with a MicroCal PEAQ-ITC instrument. Compound **1** and **2** were prepared according to the reported method.[17,18]

High-performance liquid chromatography (HPLC) was conducted on an Agilent 1260 using a Platisilph-C18 column (4.6 mm × 150 mm

Table 1. Yields of Hydrazone Products 9a−k and 10a−k[a]

entry	product	yield[b] (%)	yield[c] (%)	yield[d] (%)	product	yield[b] (%)	yield[c] (%)	yield[d] (%)
1	**9a**	94	89	0	**10a**	3	6	19
2	**9b**	90	92	0	**10b**	8	5	8
3	**9c**	92	93	6	**10c**	4	6	10
4	**9d**	93	91	6	**10d**	6	7	12
5	**9e**	90	92	0	**10e**	8	5	14
6	**9f**	92	94	0	**10f**	6	3	12
7	**9g**	91	89	0	**10g**	6	9	12
8	**9h**	88	91	0	**10h**	6	4	5
9	**9i**	94	96	0	**10i**	2	3	4
10	**9j**	94	93	0	**10j**	3	2	5
11	**9k**	93	92	0	**10k**	4	6	15

[a]The yields were determined by HPLC using anisole as an internal standard. [b]In the presence of **C1** (1.25 mM). [c]In the presence of **C2** (1.25 mM). [d]Containing KBr (7.5 mM).

https://dx.doi.org/10.1021/acs.joc.0c02792
J. Org. Chem. 2021, 86, 3943−3951

× 5 μm). The yields of products were determined by HPLC using anisole as the internal standard. The mobile phase was MeOH and H_2O and the flow rate was 1.0 μL/min. The radio (v/v) of H_2O and MeOH was 35:65 for **9a**, **9e**, **9f**, **9g**, **9i**, **9j**, and **9k**; 40:60 for **9h**; 45:55 for **7a** and **7b**; and 60:40 for **9b**, **9c**, and **9d**.

Compound M1. To a round-bottom flask were added *N*,*N*-dimethylformamide (10 mM) and then compounds **2** (0.20 g, 0.37 mmol) and 3-pyridinecarboxaldehyde **3a** (0.24 g, 2.3 mmol). The mixture was stirred at 86 °C in an oil bath for 12 h and then concentrated under reduced pressure. The resulting slurry was then triturated in acetonitrile (10 mL) and sonicated for 5 min and later filtered. The solid was washed with acetonitrile (5 mL × 3) and then dried to give compound **M1** as a pale amorphous solid (0.16 g, 50%). mp >300 °C. ^{1}H NMR (D_2O, 400 MHz): δ 8.99 (s, 3H), 8.86 (d, 3H, *J* = 6.0 Hz), 8.62 (d, 3H, *J* = 8.4 Hz), 8.04−8.08 (m, 3H), 7.36 (d, 6H, *J* = 8.0 Hz), 7.21 (d, 6H, *J* = 8.0 Hz), 6.19 (s, 3H), 5.80 (s, 6H), 2.11 (s, 3H). ^{13}C{^{1}H} NMR (D_2O, 100 MHz): δ 149.9, 144.0, 143.7, 143.3, 142.3, 130.9, 129.6, 128.8, 128.3, 86.7, 64.2, 52.1, 29.4.

HRMS (ESI) *m*/*z*: $[M - 3Br + 2H_2O]^{3+}$ calcd for $C_{41}H_{40}N_3O_5$, 218.0989; found, 218.1006.

Compound M2. Compound **M2** was prepared from the reaction of compounds **2** and **3b** in 49% yield as a pale amorphous solid according to the procedure described above for the preparation of **M1** (0.15 g, 49%). mp >300 °C (amorphous solid). ^{1}H NMR (D_2O, 400 MHz): δ 8.78 (d, 6H, *J* = 4.0 Hz), 8.02 (d, 6H, *J* = 8.0 Hz), 7.28 (d, 6H, *J* = 8.0 Hz), 7.14 (d, 6H, *J* = 8.0 Hz), 6.09 (s, 3H), 5.68 (s, 6H), 2.03 (s, 3H). ^{13}C{^{1}H} NMR (D_2O, 100 MHz): δ 160.2, 149.9, 144.5, 130.9, 129.6, 128.9, 125.5, 87.5, 63.7, 52.2, 29.4.

HRMS (ESI) *m*/*z*: $[M - 3Br + 3H_2O]^{3+}$ calcd for $C_{41}H_{42}N_3O_6$, 224.1025; found, 224.1041.

Cage C1. Compounds **M1** (8.6 mg, 10 μmol) and **4** (1.8 mg, 15 μmol) were added to D_2O (1 mL). The mixture was heated under stirring at 60 °C in an oil bath for 3 h to afford compound **C1**. It was found that, once evaporation took place, the resulting product became insoluble. Thus, **C1** was prepared in situ and characterized in solution. ^{1}H NMR (D_2O, 400 MHz): δ 9.33−9.36 (m, 6H), 8.94−9.01 (m, 6H), 8.86−8.88 (m, 6H), 8.52−8.58 (m, 6H), 8.13 (s, 6H), 7.42 (d, 12H, *J* = 4.0 Hz), 7.25 (d, 12H, *J* = 4.0 Hz), 5.85 (s, 12H), 2.12 (s, 6H). MS (ESI) *m*/*z*: $[M - 3H]^{3+}$ calcd for $C_{88}H_{75}N_{18}O_6$, 493.20; found, 493.20. $[M - 2H^+]^{4+}$ calcd for $C_{88}H_{76}N_{18}O_6$, 370.15; found, 370.15.

Cage C2. Compounds **M2** (8.6 mg, 10 μmol) and **4** (1.8 mg mM, 15 μmol) were added to D_2O (1 mL). The mixture was heated at 60 °C for 6 h to afford compound **C2**. ^{1}H NMR (D_2O, 400 MHz): δ 8.83−8.92 (m, 12H), 8.49−8.53 (m, 6H), 8.20−8.34 (m, 12H), 7.21−7.38 (m, 24H), 5.76 (s, 12H), 2.09 (s, 6H). MS (ESI) *m*/*z*: $[M + MeOH - H]^{5+}$ calcd for $C_{89}H_{81}N_{18}O_7$, 302.73; found, 302.75. $[M + 2MeOH + 3H_2O - H]^{5+}$ calcd for $C_{90}H_{91}N_{18}O_{11}$, 319.94; found, 319.95. $[M + MeOH - 2H^+]^{4+}$ calcd for $C_{89}H_{80}N_{18}O_7$, 378.16; found, 378.18. $[M - H^+]^{5+}$ calcd for $C_{88}H_{77}N_{18}O_6$, 296.32; found, 296.34; $[M - 3H^+ + H_2O]^{3+}$ calcd for $C_{88}H_{77}N_{18}O_7$, 499.54; found, 499.57.

Compounds **5**, **7a**, **7b**, **9a**−**9k**, and **10a**−**10k** have been reported in the literature. Their ^{1}H NMR data are fully consistent with those reported.

Compound 5. mp 162−163 °C (amorphous solid). ^{1}H NMR (DMSO-d_6, 400 MHz): δ 11.11−10.99 (m, 1H), 10.42 (s, 2H), 9.00−8.95 (m, 1H), 7.90−7.87 (m, 2H), 7.57−7.53 (m, 1H), 7.50−7.46 (m, 2H), 3.99−3.97 (m, 2H).[19]

Compound 7a. mp 183−184 °C (amorphous solid). ^{1}H NMR (DMSO-d_6, 400 MHz): δ 11.51 (s, 1H), 8.89−8.67 (m, 1H), 8.23−8.0 (m, 1H), 7.90−7.88 (m, 2H), 7.71−7.69 (m, 2H), 7.55−7.42 (m, 6H), 4.42−3.96 (m, 2H).[19]

Compound 7b. mp 193−194 °C (amorphous solid). ^{1}H NMR (DMSO-d_6, 400 MHz): δ 11.86−11.80 (m, 1H), 8.92−8.72 (m, 1H), 8.63 (d, 2H, *J* = 2.0 Hz), 8.23−7.92 (m, 1H), 7.89 (d, 2H, *J* = 4.0 Hz), 7.67−7.62 (m, 2H), 7.54−7.48 (m, 3H), 4.44−3.99 (m, 2H).[19]

Compound 9a. mp 200−201 °C (amorphous solid). ^{1}H NMR (DMSO-d_6, 400 MHz): δ 10.69 (s, 2H), 8.18 (s, 2H), 7.74 (d, 2H, *J* = 4.0 Hz), 7.37−7.45 (m, 6H).[20]

Compound 9b. mp 207−209 °C (amorphous solid). ^{1}H NMR (DMSO-d_6, 400 MHz): δ 10.94 (s, 2H), 8.62 (d, 4H, *J* = 2.0 Hz), 7.18 (s, 2H), 7.70 (d, 4H, *J* = 2.0 Hz).[21]

Compound 9c. mp 201−202 °C (amorphous solid). ^{1}H NMR (DMSO-d_6, 400 MHz): δ 11.12 (s, 2H), 8.91 (s, 2H), 8.57−8.59 (m, 2H), 8.17−8.24 (m, 4H), 7.45−7.49 (m, 4H).[21]

Compound 9d. mp 191−192 °C (amorphous solid). ^{1}H NMR (DMSO-d_6, 400 MHz): δ 11.04 (s, 2H), 8.57−8.59 (m, 2H), 8.23 (d, 2H, *J* = 2.0 Hz), 8.11 (d, 4H, *J* = 2.0 Hz), 7.84−7.89 (m, 2H), 7.36−7.39 (m, 2H).[20]

Compound 9e. mp 230−232 °C (amorphous solid). ^{1}H NMR (DMSO-d_6, 400 MHz): δ 10.58 (s, 2H), 8.13 (s, 2H), 7.62 (d, 4H, *J* = 4.0 Hz), 7.23 (d, 4H, *J* = 4.0 Hz), 2.33 (s, 6H).[20]

Compound 9f. mp 206−207 °C (amorphous solid). ^{1}H NMR (DMSO-d_6, 400 MHz): δ 10.6 (s, 2H), 7.98−8.13 (m, 3H), 7.54 (s, 2H), 7.47 (d, 2H, *J* = 4.0 Hz), 7.23−7.27 (m, 2H), 7.14 (d, 2H, *J* = 4.0 Hz), 2.33 (s, 6H).[22]

Compound 9g. mp 229−230 °C (amorphous solid). ^{1}H NMR (DMSO-d_6, 400 MHz): δ 10.64 (s, 2H), 8.46 (s, 2H), 7.94 (d, 2H, *J* = 2 Hz), 7.21−7.29 (m, 6H), 2.41 (s, 6H).[22]

Compound 9h. mp 193−195 °C (amorphous solid). ^{1}H NMR (DMSO-d_6, 400 MHz): δ 10.69 (s, 2H), 8.49 (s, 2H), 8.01 (s, 2H), 7.34−7.39 (m, 2H), 7.06−7.08 (m, 2H), 6.98−7.01 (m, 2H), 3.84 (s, 6H).[23]

Compound 9i. mp 236−237 °C (amorphous solid). ^{1}H NMR (DMSO-d_6, 400 MHz): δ 11.05 (s, 2H), 8.58 (s, 2H), 8.16 (s, 2H), 7.48−7.52 (m, 4H), 7.38−7.44 (m, 4H).[20]

Compound 9j. mp 221−223 °C (amorphous solid). ^{1}H NMR (DMSO-d_6, 400 MHz): δ 10.91 (s, 2H), 8.14 (s, 2H), 8.01 (s, 2H), 7.69 (d, 2H, *J* = 4.0 Hz), 7.56−7.58 (m, 2H), 7.37−7.41 (m, 2 Hz).[20]

Compound 9k. mp 234−235 °C (amorphous solid). ^{1}H NMR (DMSO-d_6, 400 MHz): δ 11.18 (s, 2H), 8.58 (s, 2H), 8.26 (d, 2H, *J* = 2.0 Hz), 8.03−8.05 (m, 2H), 7.78−7.82 (m, 2H), 7.61−7.66 (m, 2H).[24]

Compound 10a. mp 184−186 °C (amorphous solid). ^{1}H NMR (DMSO-d_6, 400 MHz): δ 10.38 (s, 1H), 8.01 (s, 1H), 7.83 (s, 1H), 7.73 (d, 4H, *J* = 2.0 Hz), 7.30−7.38 (m, 3H), 4.10 (s, 2H).[25]

Compound 10b. mp 192−193 °C (amorphous solid). ^{1}H NMR (DMSO-d_6, 400 MHz): δ 10.70 (s, 1H), 8.53 (d, 2H, *J* = 4.0 Hz), 8.27 (s, 1H), 7.80 (s, 1H), 7.71 (d, 2H, *J* = 2.0 Hz), 4.08 (s, 2H).[26]

Compound 10c. mp 192−193 °C (amorphous solid). ^{1}H NMR (DMSO-d_6, 400 MHz): δ 10.58 (s, 1H), 8.86 (s, 1H), 8.51 (d, 1H, *J* = 2.0 Hz), 8.21−8.23 (m, 2H), 7.87 (s, 1H), 7.38−7.42 (m, 1H), 4.08 (s, 2H).[26]

Compound 10d. mp 175−176 °C (amorphous solid). ^{1}H NMR (DMSO-d_6, 400 MHz): δ 10.63 (s, 1H), 8.50 (d, 1H, *J* = 2.0 Hz), 8.19−8.20 (m, 2H), 7.87 (s, 1H), 7.76−7.80 (m, 1H), 7.29−7.32 (m, 1H), 4.08 (s, 2H).[26]

Compound 10e. mp 180−182 °C (amorphous solid). ^{1}H NMR (DMSO-d_6, 400 MHz): δ 10.30 (s, 1H), 7.96 (s, 1H), 7.81 (s, 1H), 7.62 (d, 2H, *J* = 4.0 Hz), 7.19 (d, 2H, *J* = 4.0 Hz), 4.05 (s, 2H), 2.32 (s, 3H).[25]

Compound 10f. mp 185−187 °C (amorphous solid). ^{1}H NMR (DMSO-d_6, 400 MHz): δ 10.35 (s, 1H), 8.00 (s, 1H), 7.81 (s, 1H), 7.61 (s, 1H), 7.48 (d, 1H, *J* = 4.0 Hz), 7.26 (t, 1H, *J* = 4.0 Hz), 7.15 (d, 1H, *J* = 2.0 Hz), 4.07 (s, 2H), 2.32 (s, 3H).[25]

Compound 10g. mp 184−185 °C (amorphous solid). ^{1}H NMR (DMSO-d_6, 400 MHz): δ 10.32 (s, 1H), 8.14 (s, 1H), 7.95 (d, 1H, *J* = 4.0 Hz), 7.89 (s, 1H), 7.16−7.24 (m, 3H), 4.07 (s, 2H), 2.35 (s, 3H).[25]

Compound 10h. mp 186−187 °C (amorphous solid). ^{1}H NMR (DMSO-d_6, 400 MHz): δ 10.36 (s, 1H), 8.16 (s, 1H), 8.01−8.04 (m, 1H), 7.96 (s, 1H), 7.29−7.33 (m, 1H), 7.02 (d, 1H, *J* = 4.0 Hz), 6.93 (t, 1H, *J* = 4.0 Hz), 4.04 (s, 2H), 3.80 (s, 3H).[25]

Compound 10i. mp 182−184 °C (amorphous solid). ^{1}H NMR (DMSO-d_6, 400 MHz): δ 10.62 (s, 1H), 8.22−8.25 (m, 2H), 8.16 (s, 1H), 8.43−8.45 (m, 1H), 7.31−7.37 (m, 2H), 4.07 (s, 2H).[25]

Compound 10j. mp 187−189 °C (amorphous solid). ^{1}H NMR (DMSO-d_6, 400 MHz): δ 10.48 (s, 1H), 8.27 (s, 1H), 8.13 (s, 1H), 8.78 (s, 1H), 7.62 (d, 1H, *J* = 4.0 Hz), 7.48−7.51 (m, 1H), 7.29−7.33 (m, 1H), 4.05 (s, 2H).[25]

https://dx.doi.org/10.1021/acs.joc.0c02792
J. Org. Chem. 2021, 86, 3943−3951

Compound 10k. mp 212−214 °C (amorphous solid). ^{1}H NMR (DMSO-d_6, 400 MHz): δ 10.75 (s, 1H), 8.40 (d, 1H, J = 4.0 Hz), 8.23 (s, 1H), 8.17 (s, 1H), 7.97 (d, 1H, J = 4.0 Hz), 7.70 (t, 1H, J = 4.0 Hz), 7.54−7.58 (m, 1H), 4.09 (s, 2H).[25]

■ ASSOCIATED CONTENT

Supporting Information

The Supporting Information is available free of charge at https://pubs.acs.org/doi/10.1021/acs.joc.0c02792.

Experimental details, ^{1}H and ^{13}C spectra, mass spectra, ^{1}H NMR and ITC titration results, solubility data, HPLC, and calculation methods (PDF)

■ AUTHOR INFORMATION

Corresponding Authors

Dan-Wei Zhang − *Department of Chemistry, Shanghai Key Laboratory of Molecular Catalysis and Innovative Materials, Fudan University, Shanghai 200438, China;* orcid.org/0000-0003-1244-1850; Email: zhangdw@fudan.edu.cn

Zhiming Li − *Department of Chemistry, Shanghai Key Laboratory of Molecular Catalysis and Innovative Materials, Fudan University, Shanghai 200438, China*; Email: zmli@fudan.edu.cn

Zhan-Ting Li − *Department of Chemistry, Shanghai Key Laboratory of Molecular Catalysis and Innovative Materials, Fudan University, Shanghai 200438, China;* orcid.org/0000-0003-3954-0015; Email: ztli@fudan.edu.cn

Authors

Yan-Yan Xu − *Department of Chemistry, Shanghai Key Laboratory of Molecular Catalysis and Innovative Materials, Fudan University, Shanghai 200438, China*

Hong-Kun Liu − *Department of Chemistry, Shanghai Key Laboratory of Molecular Catalysis and Innovative Materials, Fudan University, Shanghai 200438, China*

Ze-Kun Wang − *Department of Chemistry, Shanghai Key Laboratory of Molecular Catalysis and Innovative Materials, Fudan University, Shanghai 200438, China*

Bo Song − *Department of Chemistry, Northwestern University, Evanston, Illinois 60208, United States;* orcid.org/0000-0002-4337-848X

Hui Wang − *Department of Chemistry, Shanghai Key Laboratory of Molecular Catalysis and Innovative Materials, Fudan University, Shanghai 200438, China*

Xiaopeng Li − *College of Chemistry and Environmental Engineering, Shenzhen University, Shenzhen, Guangdong 518055, China;* orcid.org/0000-0001-9655-9551

Complete contact information is available at: https://pubs.acs.org/10.1021/acs.joc.0c02792

Notes

The authors declare no competing financial interest.

■ ACKNOWLEDGMENTS

The work was financially supported by National Natural Science Foundation of China (nos: 21890732, 21890730 and 21921003).

■ REFERENCES

(1) (a) Cram, D. J. Molecular container compounds. *Nature* **1992**, *356*, 29−36. (b) Jasat, A.; Sherman, J. C. Carceplexes and hemicarceplexes. *Chem. Rev.* **1999**, *99*, 931−968. (c) Kubik, S. Molecular Cages and Capsules with Functionalized Inner Surfaces. *Top. Curr. Chem.* **2012**, *319*, 1−34.

(2) (a) Jin, Y.; Yu, C.; Denman, R. J.; Zhang, W. Recent advances in dynamic covalent chemistry. *Chem. Soc. Rev.* **2013**, *42*, 6634−6654. (b) Zhang, G.; Mastalerz, M. Organic cage compounds from shape-persistency to function. *Chem. Soc. Rev.* **2014**, *43*, 1934−1947. (c) Briggs, M. E.; Cooper, A. I. A Perspective on the Synthesis, Purification, and Characterization of Porous Organic Cages. *Chem. Mater.* **2017**, *29*, 149−157. (d) Jordan, J. H.; Gibb, B. C. Molecular containers assembled through the hydrophobic effect. *Chem. Soc. Rev.* **2015**, *44*, 547−585. (e) Amendola, V.; Bergamaschi, G.; Miljkovic, A. Azacryptands as molecular cages for anions and metal ions. *Supramol. Chem.* **2018**, *30*, 236−242. (f) Elemans, J. A. A. W.; Nolte, R. J. M. Porphyrin cage compounds based on glycoluril-from enzyme mimics to functional molecular machines. *Chem. Commun.* **2019**, *55*, 9590−9605. (g) Acharyya, K.; Mukherjee, P. S. Organic Imine Cages: Molecular Marriage and Applications. *Angew. Chem., Int. Ed.* **2019**, *58*, 8640−8653. (h) Akine, S.; Sakata, Y. Control of Guest Binding Kinetics in Macrocycles and Molecular Cages. *Chem. Lett.* **2020**, *49*, 428−441. (i) Duan, H.; Li, Y.; Li, Q.; Wang, P.; Liu, X.; Cheng, L.; Yu, Y.; Cao, L. Host-Guest Recognition and Fluorescence of a Tetraphenylethene-Based Octacationic Cage. *Angew. Chem., Int. Ed.* **2020**, *59*, 10101−10110. (j) Liu, Y.; Zhao, W.; Chen, CH; Flood, AH Chloride capture using a C-H hydrogen-bonding cage. *Science* **2019**, *365*, 159−161.

(3) Mastalerz, M. Porous Shape-Persistent Organic Cage Compounds of Different Size, Geometry, and Function. *Acc. Chem. Res.* **2018**, *51*, 2411−2422.

(4) (a) Roy, N.; Bruchmann, B.; Lehn, J.-M. DYNAMERS: dynamic polymers as self-healing materials. *Chem. Soc. Rev.* **2015**, *44*, 3786−3807. (b) Corbett, P. T.; Leclaire, J.; Vial, L.; West, K. R.; Wietor, J.-L.; Sanders, J. K. M.; Otto, S. Dynamic Combinatorial Chemistry. *Chem. Rev.* **2006**, *106*, 3652−3711.

(5) (a) Mastalerz, M. Shape-persistent organic cage compounds by dynamic covalent bond formation. *Angew. Chem., Int. Ed.* **2010**, *49*, 5042−5053. (b) Jin, Y.; Wang, Q.; Taynton, P.; Zhang, W. Dynamic Covalent Chemistry Approaches Toward Macrocycles, Molecular Cages, and Polymers. *Acc. Chem. Res.* **2014**, *47*, 1575−1586. (c) Wierzbicki, M.; Glowacka, A. A.; Szymanski, M. P.; Szumna, A. A. A chiral member of the family of organic hexameric cages. *Chem. Commun.* **2017**, *53*, 5200−5203. (d) Ono, K.; Iwasawa, N. Dynamic Behavior of Covalent Organic Cages. *Chem. -Eur. J.* **2018**, *24*, 17856−17868.

(6) (a) Zheng, X.; Zhang, Y.; Wu, G.; Liu, J.-R.; Cao, N.; Wang, L.; Wang, Y.; Li, X.; Hong, X.; Yang, C.; Li, H. Temperature-dependent self-assembly of a purely organic cage in water. *Chem. Commun.* **2018**, *54*, 3138−3141. (b) Wu, G.; Wang, C.-Y.; Jiao, T.; Zhu, H.; Huang, F.; Li, H. Controllable Self-Assembly of Macrocycles in Water for Isolating Aromatic Hydrocarbon Isomers. *J. Am. Chem. Soc.* **2018**, *140*, 5955−5961.

(7) (a) Schmidt, A.; Casini, A.; Kühn, F. E. Self-assembled M_2L_4 coordination cages: Synthesis and potential applications. *Coord. Chem. Rev.* **2014**, *275*, 19−36. (b) Li, H.; Yao, Z.-J.; Liu, D.; Jin, G.-X. Multicomponent coordination-driven self-assembly toward heterometallic macrocycles and cages. *Coord. Chem. Rev.* **2015**, *293*−*294*, 139−157. (c) Ward, M. D.; Hunter, C. A.; Williams, N. H. Guest binding and catalysis in the cavity of a cubic coordination cage. *Chem. Lett.* **2017**, *46*, 2−9. (d) Bloch, W. M.; Clever, G. H. Integrative self-sorting of coordination cages based on "naked" metal ions. *Chem. Commun.* **2017**, *53*, 8506−8516. (e) Ward, M. D.; Hunter, C. A.; Williams, N. H. Coordination Cages Based on Bis(pyrazolylpyridine) Ligands: Structures, Dynamic Behavior, Guest Binding, and Catalysis. *Acc. Chem. Res.* **2018**, *51*, 2073−2082. (f) Tan, C.; Chu, D.; Tang, X.; Liu, Y.; Xuan, W.; Cui, Y. Supramolecular Coordination Cages for Asymmetric Catalysis. *Chem.—Eur. J.* **2019**, *25*, 662−672. (g) Fang, Y.; Powell, J. A.; Li, E.; Wang, Q.; Perry, Z.; Kirchon, A.; Yang, X.; Xiao, Z.; Zhu, C.; Zhang, L.; Huang, F.; Zhou, H.-C. Catalytic reactions within the cavity of coordination cages. *Chem. Soc. Rev.* **2019**, *48*, 4707−4730. (h) Severinsen, R. J.; Rowlands, G. J.; Plieger, P. G. Coordination

cages in catalysis. *J. Inclusion Phenom. Macrocyclic Chem.* **2020**, *96*, 29−42.

(8) (a) Uribe-Romo, F. J.; Doonan, C. J.; Furukawa, H.; Oisaki, K.; Yaghi, O. M. Crystalline Covalent Organic Frameworks with Hydrazone Linkages. *J. Am. Chem. Soc.* **2011**, *133*, 11478−11481. (b) Ding, S.-Y.; Cui, X.-H.; Feng, J.; Lu, G.; Wang, W. Facile synthesis of -C=N- linked covalent organic frameworks under ambient conditions. *Chem. Commun.* **2017**, *53*, 11956−11959. (c) Liang, R.-R.; Xu, S.-Q.; Qi, Q.-Y.; Zhao, X. Fabricating Organic Nanotubes through Selective Disassembly of Two-Dimensional Covalent Organic Frameworks. *J. Am. Chem. Soc.* **2020**, *142*, 70−74.

(9) (a) Tian, J.; Chen, L.; Zhang, D.-W.; Liu, Y.; Li, Z.-T. Supramolecular organic frameworks: engineering periodicity in water through host-guest chemistry. *Chem. Commun.* **2016**, *52*, 6351−6362. (b) Yang, B.; Zhang, X.-D.; Li, J.; Tian, J.; Wu, Y.-P.; Yu, F.-X.; Wang, R.; Wang, H.; Zhang, D.-W.; Liu, Y.; Zhou, L.; Li, Z.-T. In Situ Loading and Delivery of Short Single- and Double-Stranded DNA by Supramolecular Organic Frameworks. *CCS Chem.* **2019**, *1*, 156−165. (c) Yan, M.; Liu, X.-B.; Gao, Z.-Z.; Wu, Y.-P.; Hou, J.-L.; Wang, H.; Zhang, D.-W.; Liu, Y.; Li, Z.-T. A pore-expanded supramolecular organic framework and its enrichment of photosensitizers and catalysts for visible-light-induced hydrogen production. *Org. Chem. Front.* **2019**, *6*, 1698−1704. (d) Wu, Y.-P.; Wang, Z.-K.; Wang, H.; Zhang, D.-W.; Zhao, X.; Li, Z.-T. Self-Assembly of a Highly Fluorescent Three-Dimensional Supramolecular Organic Framework and Selective Sensing for Picric Acid. *Acta Chim. Sin.* **2019**, *77*, 735−740. (e) Lin, J.-L.; Wang, Z.-K.; Xu, Z.-Y.; Wei, L.; Zhang, Y.-C.; Wang, H.; Zhang, D.-W.; Zhou, W.; Zhang, Y.-B.; Liu, Y.; Li, Z.-T. Water-Soluble Flexible Organic Frameworks That Include and Deliver Proteins. *J. Am. Chem. Soc.* **2020**, *142*, 3577−3582. (f) Gao, Z.-Z.; Wang, Z.-K.; Wei, L.; Yin, G.; Tian, J.; Liu, C.-Z.; Wang, H.; Zhang, D.-W.; Zhang, Y.-B.; Li, X.; Liu, Y.; Li, Z.-T. Water-Soluble 3D Covalent Organic Framework that Displays an Enhanced Enrichment Effect of Photosensitizers and Catalysts for the Reduction of Protons to H_2. *ACS Appl. Mater. Interfaces* **2020**, *12*, 1404−1411.

(10) (a) Lei, Y.; Shen, L.; Liu, J.-R.; Jiao, T.; Zhang, Y.; Zhang, C.; Tong, L.; Hong, X.; Pan, Y.; Li, H. A diquat-containing macrocyclic anion acceptor in pure water. *Chem. Commun.* **2019**, *55*, 8297−8300. (b) Chen, Q.; Chen, L.; Wang, C.-Y.; Jiao, T.; Pan, Y.; Li, H. Ultramacrocyclization via selective catenation in water. *Chem. Commun.* **2019**, *55*, 13108−13111. (c) Shen, L.; Cao, N.; Tong, L.; Zhang, X.; Wu, G.; Jiao, T.; Yin, Q.; Zhu, J.; Pan, Y.; Li, H. Dynamic Covalent Self-Assembly Based on Oxime Condensation. *Angew. Chem., Int. Ed.* **2018**, *57*, 16486−16490.

(11) (a) Neira, I.; Blanco-Gómez, A.; Quintela, J. M.; García, M. D.; Peinador, C. Dissecting the "Blue Box": Self-Assembly Strategies for the Construction of Multipurpose Polycationic Cyclophanes. *Acc. Chem. Res.* **2020**, *53*, 2336−2346. (b) Blanco-Gómez, A.; Fernández-Blanco, Á.; Blanco, V.; Rodríguez, J.; Peinador, C.; García, M. D. Thinking Outside the "Blue Box": Induced Fit within a Unique Self-Assembled Polycationic Cyclophane. *J. Am. Chem. Soc.* **2019**, *141*, 3959−3964.

(12) Tian, J.; Ding, Y.-D.; Zhou, T.-Y.; Zhang, K.-D.; Zhao, X.; Wang, H.; Zhang, D.-W.; Liu, Y.; Li, Z.-T. Self-Assembly of Three-Dimensional Supramolecular Polymers through Cooperative Tetrathiafulvalene Radical Cation Dimerization. *Chem.—Eur. J.* **2014**, *20*, 575−584.

(13) (a) Becke, A. D. Density-functional thermochemistry. III. The role of exact exchange. *J. Chem. Phys.* **1993**, *98*, 5648−5652. (b) Stephens, P. J.; Devlin, F. J.; Chabalowski, C. F.; Frisch, M. J. Ab Initio Calculation of Vibrational Absorption and Circular Dichroism Spectra Using Density Functional Force Fields. *J. Phys. Chem.* **1994**, *98*, 11623−11627. (c) Lee, C.; Yang, W.; Parr, R. G. Development of the Colle-Salvetti correlation-energy formula into a functional of the electron density. *Phys. Rev. B: Condens. Matter Mater. Phys.* **1988**, *37*, 785−789.

(14) Frisch, M. J.; et al. *Gaussian 09*, Revision D.01; Gaussian, Inc.: Wallingford, CT, 2009.

(15) Marenich, A. V.; Cramer, C. J.; Truhlar, D. G. Universal Solvation Model Based on Solute Electron Density and on a Continuum Model of the Solvent Defined by the Bulk Dielectric Constant and Atomic Surface Tensions. *J. Phys. Chem. B* **2009**, *113*, 6378−6396.

(16) (a) Diederich, F.; Dick, K. A new water-soluble macrocyclic host of the cyclophane type: host-guest complexation with aromatic guests in aqueous solution and acceleration of the transport of arenes through an aqueous phase. *J. Am. Chem. Soc.* **1984**, *106*, 8024−8036. (b) Meyer, E. A.; Castellano, R. K.; Diederich, F. Interactions with aromatic rings in chemical and biological recognition. *Angew. Chem., Int. Ed.* **2003**, *42*, 1210−1250. (c) Maurizot, V.; Yoshizawa, M.; Kawano, M.; Fujita, M. Control of molecular interactions by the hollow of coordination cages. *Dalton Trans.* **2006**, 2750−2756. (d) Ajami, D.; Rebek, J., Jr. More Chemistry in Small Spaces. *Acc. Chem. Res.* **2013**, *46*, 990−999. (e) Cullen, W.; Metherell, A. J.; Wragg, A. B.; Taylor, C. G. P.; Williams, N. H.; Ward, M. D. Catalysis in a Cationic Coordination Cage Using a Cavity-Bound Guest and Surface-Bound Anions: Inhibition, Activation, and Autocatalysis. *J. Am. Chem. Soc.* **2018**, *140*, 2821−2828. (f) Yang, B.; Wang, H.; Zhang, D. W.; Li, Z. T. Water-Soluble Three-Dimensional Polymers: Non-Covalent and Covalent Synthesis and Functions. *Chin. J. Chem.* **2020**, *38*, 970−980. (g) Zhang, Y.-M.; Xu, Q.-Y.; Liu, Y. Molecular recognition and biological application of modified β-cyclodextrins. *Sci. China Chem.* **2019**, *62*, 549−560. (h) Kamatham, N.; Da Silva, J. P.; Givens, R. S.; Ramamurthy, V. Melding Caged Compounds with Supramolecular Containers: Photogeneration and Miscreant Behavior of the Coumarylmethyl Carbocation. *Org. Lett.* **2017**, *19*, 3588−3591.

(17) De Silva, A.; Lee, J.-K.; André, X.; Felix, N. M.; Cao, H. B.; Deng, H.; Ober, C. K. Study of the Structure-Properties Relationship of Phenolic Molecular Glass Resists for Next Generation Photolithography. *Chem. Mater.* **2008**, *20*, 1606−1613.

(18) Bähring, S.; Larsen, K. R.; Supur, M.; Nielsen, K. A.; Poulsen, T.; Ohkubo, K.; Marlatt, C. W.; Miyazaki, E.; Takimiya, K.; Flood, A. H.; Fukuzumi, S.; Jeppesen, J. O. Ionic manipulation of charge-transfer and photodynamics of [60]fullerene confined in pyrrolo-tetrathiafulvalene cage. *Chem. Commun.* **2017**, *53*, 9898−9901.

(19) Nikalje, A. P. G.; Shaikh, A. N.; Shaikh, S. I.; Kalam Khan, F. A.; Sangshetti, J. N.; Shinde, D. B. Microwave assisted synthesis and docking study of N-(2-oxo-2-(4oxo-2-substituted thiazolidin-3ylamino)ethyl)benzamide derivatives as anticonvulsant agents. *Bioorg. Med. Chem. Lett.* **2014**, *24*, 5558−5562.

(20) Wen, J.; Yang, C.-T.; Jiang, T.; Hu, S.; Yang, T.-Z.; Wang, X.-L. Efficient Synthesis of 1,5-Disubstituted Carbohydrazones Using K2CO3 As a Carbonyl Donor. *Org. Lett.* **2014**, *16*, 2398−2401.

(21) Hoque, M. N.; Utsab, M.; Gopal, D. Discrepancy in anion coordination directed by isomeric pyridine-urea receptors: Solid state recognition of hydrated anions. *Polyhedron* **2016**, *119*, 307−316.

(22) Russell, C. C.; Stevens, A.; Pi, H.; Khazandi, M.; Ogunniyi, A. D.; Young, K. A.; Baker, J. R.; McCluskey, S. N.; Page, S. W.; Trott, D. J.; McCluskey, A. Gram-Positive and Gram-Negative Antibiotic Activity of Asymmetric and Monomeric Robenidine Analogues. *ChemMedChem* **2018**, *13*, 2573−2580.

(23) Li, Z.; Zhu, W.; Yu, J.; Ma, X.; Lu, Z.; Xiao, S. Green Synthetic Method for 1,5-Disubstituted Carbohydrazones. *Synth. Commun.* **2006**, *36*, 2613−2619.

(24) Iqbal, S.; Saleem, M.; Azim, M. K.; Taha, M.; Salar, U.; Khan, K. M.; Perveen, S.; Choudhary, M. I. Carbohydrazones as new class of carbonic anhydrase inhibitors: Synthesis, kinetics, and ligand docking studies. *Bioorg. Chem.* **2017**, *72*, 89−101.

(25) Mrdjan, G. S.; Matijević, B. M.; Vastag, G. G.; Božić, A. R.; Marinković, A. D.; Milčić, M. K.; Stojiljković, I. N. Synthesis, solvent interactions and computational study of monocarbohydrazones. *Chem. Pap.* **2020**, *74*, 2653−2674.

(26) Božić, A. R.; Filipovic, N. R.; Verbic, T. Z.; Milcic, M. K.; Todorovic, T. R.; Cvijetic, I. N.; Klisuric, O. R.; Radisic, M. M.; Marinkovic, A. D. A detailed experimental and computational study of monocarbohydrazones. *Arabian J. Chem.* **2020**, *13*, 932−953.

https://dx.doi.org/10.1021/acs.joc.0c02792
J. Org. Chem. 2021, 86, 3943−3951